Ab initio simulations of light propagation in silver cluster nanostructures

Polina G. Lisinetskaya
Fachbereich Physik, Freie Universität Berlin, Arnimallee 14, D-14195 Berlin, Germany

Roland Mitrić*
Institut für Physikalische und Theoretische Chemie, Universität Würzburg, D-97074 Würzburg, Germany
(Received 28 October 2013; revised manuscript received 20 December 2013; published 28 January 2014)

We present a theoretical approach for the simulation of the optical response and light propagation in aggregates and in ordered arrays of small noble-metal clusters with discrete electronic structure. We construct the Hamiltonian for the aggregate system based on the time-dependent density functional theory electronic states of the individual subunits and describe the interaction between them using the dipole approximation. The time evolution of the aggregate under the influence of the external electric field is obtained from the numerical solution of the time-dependent Schrödinger equation with the coupled excitonic Hamiltonian. For each subunit, the time-dependent dipole moment is calculated using the reduced density matrix formalism. Such quantum-mechanically determined dipole moments are used to simulate the spatiotemporal distribution of the electric field produced by the array. Additionally, we introduce an approximate self-consistent iterative approach to treat arrays consisting of many subunits which are of interest in the context of nanoplasmonics, nano-optical applications, and development of light-harvesting materials. The developed methodology is illustrated first on the example of Ag_2 and Ag_8 cluster pairs. Subsequently, light propagation in a triangular-shaped array consisting of six Ag_8 clusters is simulated.

DOI: 10.1103/PhysRevB.89.035433 PACS number(s): 36.40.−c

I. INTRODUCTION

In recent decades, nanosized noble-metal clusters and their aggregates have become the subject of intense experimental and theoretical research due to their unique chemical, electronic, and optical properties as compared to their bulk counterparts [1–13]. It has been recognized that nanosized noble-metal particles exhibit collective oscillations of conduction electrons, known as plasmons, which cause strong absorption of light in the visible region [14,15] that is absent in individual atoms or bulk material. Since excitation of plasmon resonance is strongly affected by shape, size, and dielectric environment of the nanoparticle [16,17], these parameters can be adjusted for application at desired wavelength. The strong local field near the surface of a plasmonic particle can enhance the optical response of a molecule placed in its vicinity, as it has been demonstrated in surface-enhanced Raman spectroscopy [18] or metal-enhanced fluorescence [19] experiments. In addition, arrays of closely spaced metal nanoparticles can guide electromagnetic energy due to strong near-field coupling between neighboring subunits [20]. All the above-mentioned properties make noble-metal nanoparticles and their assemblies promising building blocks for various optical and photonic applications ranging from subwavelength imaging and energy transport [21–23] to biosensing and single-molecule detection [6,24,25].

Continued reduction of the size of nanoparticles leads eventually to subnanometer-sized metal clusters with molecularlike discrete energy levels. In this size range, the plasmonic absorption band of a nanoparticle transforms into discrete electronic transitions strongly dependent on the number of atoms in the cluster and its geometrical shape [5,26]. Thus, the optical and electronic properties of these particles do not scale with cluster size, and adding even a single atom or changing the structure can dramatically affect the properties of the cluster [3,27–29]. Apart from that, aggregates of subnanometer metal clusters demonstrate novel functionalities exceeding those of individual constituents [30].

One of the exciting possibilities to exploit such aggregates for various applications is to control light propagation and localization, aiming to deliver excitation to a desired spatial point at a desired instant of time. By combining adaptive control with nano-optics, a subwavelength dynamic localization of light has been demonstrated experimentally in specifically designed aggregates of silver nanoparticles [31,32]. Parallel to the experimental developments, considerable attention has been devoted to the theoretical simulation of light propagation and localization in noble-metal nanostructures. By now, several theoretical approaches have been demonstrated including the finite-difference time-domain method (FDTD) [33–35], the boundary elements method (BEM) [36], the discrete-dipole approximation (DDA) [37], the extended Mie theory [21,38,39], and the quasistatic approximation to Maxwell equations [40,41] applied to 10–100 nanometer-sized nanoparticles and their aggregates. Additionally, the above-mentioned methods for solving the Maxwell equations were coupled to the Bloch [42–44], Schrödinger [45], and Liouville [46] equations for the description of the quantum dynamics in complex systems consisting of nanoparticles interacting with molecules or atomic systems. The main drawback of the latter group of methods is that they treat atoms or molecules in the system as few-level quantum systems with degenerate excited states and thus do not describe the electronic structure of the individual systems and their interaction realistically. However, this description is mandatory both for the interpretation of experimental results as well as for proposing novel systems and experiments.

*Also at Fachbereich Physik, Freie Universität Berlin, Arnimallee 14, D-14195 Berlin, Germany; roland.mitric@uni-wuerzburg.de

In this study, we present methods for simulation of optical response and light propagation in ordered arrays of subnanometer molecularlike metal clusters including a large number of nondegenerate excited electronic states obtained from time-dependent density functional theory (TDDFT). We treat the whole array as a complex quantum system and propagate the time-dependent Schrödinger equation (TDSE) under the action of an external laser pulse in the manifold of the system eigenstates. Subsequently, we employ the reduced density matrix formalism to retrieve time-dependent dipole moments of each individual constituent. Finally, using methods of classical electrodynamics we calculate the temporal and spatial distribution of the electric field produced by the array, treating each subunit as a point dipole emitter with the quantum-mechanically determined time-dependent dipole moment. Since inclusion of numerous excited states per cluster leads to computational overburdening, we develop an approximate self-consistent iterative approach to treat large metal-cluster arrays. This approach is based on the iterative solution of the TDSE for each cluster separately under the action of the external laser field and the electric fields produced by the other clusters in the array. The described methods are first applied to an Ag_2 cluster pair since for this system more accurate calculations using the correlated *ab initio* approximate coupled cluster singles and doubles (CC2) method [47] can be performed. Subsequently, a system with more complex energy level structure, namely, the Ag_8 cluster pair, is investigated. For both cases, the validity of the approximate iterative approach is examined. Finally, using the iterative approach, we simulate the spatiotemporal distribution of the electric field produced by a triangular-shaped array consisting of six Ag_8 clusters.

The paper is structured as follows: In Sec. II, the theoretical approach is described and the working equations are derived; in Sec. III, computational details are specified. The results are presented and discussed in Sec. IV, and in Sec. V conclusions and outlook are given.

II. THEORY

In this section, we introduce the theoretical methodology for the simulation of optical response and light propagation in silver-cluster arrays by combining the *ab initio* description of the electronic structure of individual clusters with classical electrodynamics simulations of the electric field distributions. The section is structured in the following way: In Sec. II A, the construction of an excitonic Hamiltonian of a cluster array is discussed, and in Sec. II B, eigenenergies and eigenfunctions of the external-field-free part of the excitonic Hamiltonian are determined. In Sec. II C, the approach to the simulation of the time-dependent response of the cluster array is given and an expression for the spatiotemporal distribution of the electric field produced by the array is derived. The method to obtain transition dipole moments in the frame of TDDFT is discussed in Sec. II D. Finally, in Sec. II E, the approximate iterative approach for application to large arrays is presented.

A. Exciton Hamiltonian for the cluster array

We assume that our system is composed of an array of N weakly interacting metal clusters. The Hamiltonian H_I of the Ith cluster is built up from the electronic Hamiltonian $\hat{\mathrm{H}}_0^{(I)}$, which can be constructed based on the TDDFT calculations as described in Sec. II D, and the electromagnetic perturbation arising from the external electric field and the response of other clusters in the array:

$$\hat{\mathrm{H}}_I = \hat{\mathrm{H}}_0^{(I)} - \hat{\boldsymbol{\mu}}_I \cdot \left(\sum_{J \neq I} \boldsymbol{\varepsilon}_J(\mathbf{r},t) + \boldsymbol{\varepsilon}_{\mathrm{ext}}(\mathbf{r},t) \right). \tag{1}$$

Here, $\hat{\boldsymbol{\mu}}_I$ is the electronic dipole moment operator of the Ith cluster, $\boldsymbol{\varepsilon}_{\mathrm{ext}}(\mathbf{r},t)$ is the external electric field strength, $\boldsymbol{\varepsilon}_J(\mathbf{r},t)$ is the electric field produced by the electromagnetic response of the Jth cluster. Notably, the term $-\hat{\boldsymbol{\mu}}_I \cdot \sum \boldsymbol{\varepsilon}_J(\mathbf{r},t)$ represents the cluster-cluster interaction, which within the considered approach is assumed to be purely electromagnetic. The total electronic Hamiltonian ($\hat{\mathrm{H}}$) of the cluster array with N subunits is constructed from the Hamiltonians of individual components (1) as

$$\begin{aligned}\hat{\mathrm{H}} = &\sum_{I=1}^{N} \hat{\mathrm{H}}_0^{(I)} \otimes \mathbf{I}^{(I)} - \sum_{I=1}^{N} \sum_{J>I} \hat{\boldsymbol{\mu}}_I \otimes \mathbf{I}^{(I,J)} \cdot \boldsymbol{\varepsilon}_J(\mathbf{r},t) \\ &- \sum_{I=1}^{N} \hat{\boldsymbol{\mu}}_I \otimes \mathbf{I}^{(I)} \cdot \boldsymbol{\varepsilon}_{\mathrm{ext}}(\mathbf{r},t),\end{aligned} \tag{2}$$

where $\mathbf{I}^{(I)}$ and $\mathbf{I}^{(I,J)}$ are the identity operators acting on the electrons of all clusters in the array, except cluster I or I and J, respectively.

The electronic coupling between the clusters $\hat{\boldsymbol{\mu}}_I \cdot \boldsymbol{\varepsilon}_J(\mathbf{r},t)$ in the lowest approximation can be modeled by dipole-dipole interaction terms. This leads to the excitonic Hamiltonian which does not take into account the possibility of charge-transfer excitations between individual subunits. However, since in our simulations the distance between the clusters will be kept relatively large, such charge-transfer excitations are unlikely to contribute to the optical properties of the array. For example, for the Ag_2 cluster pair at $10a_0$ separation, which serves as a benchmark system in our simulations, the correlated *ab initio* CC2 calculations predict no charge-transfer excitation below 4.9 eV, which is considerably higher than the frequency of the external laser pulse (2.98 eV). Thus, the total Hamiltonian describing the array with fixed nuclei irradiated by the external electric field reads as

$$\begin{aligned}\hat{\mathrm{H}} = &\sum_{I=1}^{N} \hat{\mathrm{H}}_0^{(I)} \otimes \mathbf{I}^{(I)} \\ &+ \sum_{I}^{N} \sum_{J>I} \left(\frac{\hat{\boldsymbol{\mu}}_I \hat{\boldsymbol{\mu}}_J}{r_{IJ}^3} - \frac{3}{r_{IJ}^5} (\hat{\boldsymbol{\mu}}_I \mathbf{r}_{IJ})(\hat{\boldsymbol{\mu}}_J \mathbf{r}_{IJ}) \right) \otimes \mathbf{I}^{(I,J)} \\ &- \sum_{I=1}^{N} \hat{\boldsymbol{\mu}}_I \otimes \mathbf{I}^{(I)} \cdot \boldsymbol{\varepsilon}_{\mathrm{ext}}(\mathbf{r},t) \\ = &\hat{\mathrm{H}}_{\mathrm{arr}} - \sum_{I=1}^{N} \hat{\boldsymbol{\mu}}_I \otimes \mathbf{I}^{(I)} \cdot \boldsymbol{\varepsilon}_{\mathrm{ext}}(\mathbf{r},t).\end{aligned} \tag{3}$$

Here, $\mathbf{r}_{IJ}$ is a vector pointing from the charge center of the Ith cluster to the center of the Jth one ($\mathbf{r}_{IJ} = \mathbf{R}_J - \mathbf{R}_I$), $\mathbf{R}_I$ is the position of the charge center of the Ith cluster,

and $\hat{\mathrm{H}}_{\mathrm{arr}}$ denotes the external-field-free Hamiltonian of the cluster array. The form of the Hamiltonian (3) suggests that the natural basis for solving the TDSE is the basis spanned by the eigenfunctions of $\hat{\mathrm{H}}_{\mathrm{arr}}$ since this operator is fully determined by properties of individual clusters and their spatial configuration. Thus, once calculated, the eigenfunctions and eigenvalues of this Hamiltonian can be used as a basis to simulate the optical response of the cluster array to various external electric fields.

B. Eigenfunctions and eigenenergies of the external field-free Hamiltonian $\hat{\mathrm{H}}_{\mathrm{arr}}$

As a basis for the representation of the coupled array Hamiltonian $\hat{\mathrm{H}}_{\mathrm{arr}}$, we employ the product-state basis constructed from the individual cluster eigenfunctions:

$$|\phi_{ij\ldots z}\rangle = \left|\Psi_i^{(1)}\right\rangle \otimes \left|\Psi_j^{(2)}\right\rangle \otimes \cdots \otimes \left|\Psi_z^{(N)}\right\rangle, \tag{4}$$

where each eigenfunction $|\Psi_i^{(I)}\rangle$ satisfies the time-independent Schrödinger equation $\hat{\mathrm{H}}_0^{(I)}|\Psi_i^{(I)}\rangle = E_i^{(I)}|\Psi_i^{(I)}\rangle$ with $E_i^{(I)}$ representing the ith electronic state energy of the Ith cluster, and the indices $i, j, \ldots, z$ go over all included electronic states for each individual cluster. In this basis, the Hamiltonian $\hat{\mathrm{H}}_{\mathrm{arr}}$ can be represented by a supermatrix with the elements

$$(\mathrm{H}_{\mathrm{arr}})_{ij\ldots z,i'j'\ldots z'} = \langle\phi_{ij\ldots z}|\hat{\mathrm{H}}_{\mathrm{arr}}|\phi_{i'j'\ldots z'}\rangle. \tag{5}$$

Due to the orthogonality of the single-cluster eigenfunctions $\langle\Psi_{i'}^{(I)}|\Psi_i^{(I)}\rangle = \delta_{ii'}$, all matrix elements with three or more different indices in the set $ij\ldots z$ are zero. The diagonal matrix elements have the following form:

$$\begin{aligned}(\mathrm{H}_{\mathrm{arr}})_{ij\ldots z,ij\ldots z} &= E_i^{(1)} + E_j^{(2)} + \cdots + E_z^{(N)} \\ &\quad + \sum_{I=1}^{N}\sum_{J>I}\left[\frac{1}{r_{IJ}^3}\boldsymbol{\mu}_{k_Ik_I}^{(I)}\cdot\boldsymbol{\mu}_{k_Jk_J}^{(J)}\right. \\ &\quad \left. - \frac{3}{r_{IJ}^5}\left(\boldsymbol{\mu}_{k_Ik_I}^{(I)}\cdot\mathbf{r}_{IJ}\right)\left(\boldsymbol{\mu}_{k_Jk_J}^{(J)}\cdot\mathbf{r}_{IJ}\right)\right],\end{aligned} \tag{6}$$

where k_I is the the index of the electronic state of the Ith cluster. For example, for a particular basis function $|\phi_{ij\ldots z}\rangle$, the indices have the values $k_1 = i$, $k_2 = j, \ldots, k_N = z$. The $\boldsymbol{\mu}_{k_Ik_I}^{(I)} = \langle\Psi_i^{(I)}|\hat{\boldsymbol{\mu}}_I|\Psi_i^{(I)}\rangle$ is the permanent dipole moment of the Ith cluster in the state i. The nondiagonal elements of the matrix $(\mathrm{H}_{\mathrm{arr}})$ with only one different index are

$$\begin{aligned}&(\mathrm{H}_{\mathrm{arr}})_{ij\ldots k_I\ldots z,ij\ldots k_I'\ldots z} \\ &= \sum_{J=1}^{N}\left[\frac{1}{r_{IJ}^3}\boldsymbol{\mu}_{k_Ik_I'}^{(I)}\cdot\boldsymbol{\mu}_{k_Jk_J}^{(J)} - \frac{3}{r_{IJ}^5}\left(\boldsymbol{\mu}_{k_Ik_I'}^{(I)}\cdot\mathbf{r}_{IJ}\right)\left(\boldsymbol{\mu}_{k_Jk_J}^{(J)}\cdot\mathbf{r}_{IJ}\right)\right].\end{aligned} \tag{7}$$

Here, $\boldsymbol{\mu}_{k_Ik_I'}^{(I)} = \langle\Psi_i^{(I)}|\hat{\boldsymbol{\mu}}_I|\Psi_{i'}^{(I)}\rangle$ is the transition dipole moment between the states i and i' of the Ith cluster. Finally, the elements of the matrix $(\mathrm{H}_{\mathrm{arr}})$ with two different indices read as

$$\begin{aligned}&(\mathrm{H}_{\mathrm{arr}})_{ij\ldots k_I\ldots k_J\ldots z,ij\ldots k_I'\ldots k_J'\ldots z} \\ &= \frac{1}{r_{IJ}^3}\boldsymbol{\mu}_{k_Ik_I'}^{(I)}\cdot\boldsymbol{\mu}_{k_Jk_J'}^{(J)} - \frac{3}{r_{IJ}^5}\left(\boldsymbol{\mu}_{k_Ik_I'}^{(I)}\cdot\mathbf{r}_{IJ}\right)\left(\boldsymbol{\mu}_{k_Jk_J'}^{(J)}\cdot\mathbf{r}_{IJ}\right).\end{aligned} \tag{8}$$

The diagonalization of the field-free excitonic Hamiltonian $\hat{\mathrm{H}}_{\mathrm{arr}}$ gives rise to the set of excitonic states with eigenenergies E_p and eigenfunctions $|\psi_p\rangle$ which in the tensor basis (4) can be expanded as

$$\begin{aligned}|\psi_p\rangle &= \sum_{ij\ldots z} C_{ij\ldots z}^p|\phi_{ij\ldots z}\rangle \\ &= \sum_{ij\ldots z} C_{ij\ldots z}^p\left|\Psi_i^{(1)}\right\rangle \otimes \left|\Psi_j^{(2)}\right\rangle \otimes \cdots \otimes \left|\Psi_z^{(N)}\right\rangle.\end{aligned} \tag{9}$$

C. Time-dependent response of the cluster array to the external electromagnetic field

In order to simulate the electromagnetic response of cluster arrays induced by external laser fields, the electronic dynamics of the whole system can be calculated fully quantum mechanically by solving the TDSE. Our aim is to develop a general methodology for the simulation of the electromagnetic response of cluster arrays with arbitrary shapes and sizes. The only restriction we make is that the individual components are much smaller than the wavelength of the light used for excitation, and are typically in the range of 1–10 nm. This allows us to consider each individual component as a dipole emitter. The response of the whole nanostructure with arbitrary size is then modeled by taking into account the spatial variation of electromagnetic field phase at the positions of individual clusters. Within these restrictions, the interaction of each component with the external field is described by a dipole term $-\hat{\boldsymbol{\mu}}_I\cdot\boldsymbol{\varepsilon}_0(t)(e^{i(\mathbf{k}_\omega\cdot\mathbf{R}_I-\omega t)} + \text{c.c.})$ where the spatial variation of the external electric field over the whole array is taken into account by the position-dependent phase, and $\boldsymbol{\varepsilon}_0(t)$ represents the time envelope of the field.

As a basis for the solution of the TDSE, it is convenient to employ the excitonic eigenfunctions defined in Eq. (9). Thus, the total time-dependent wave function of the cluster array can be expanded into the excitonic eigenstates as $|\Phi(t)\rangle = \sum_p D_p(t)e^{-iE_pt}|\psi_p\rangle$, where $D_p(t)$ are the time-dependent coefficients which are determined by solving the following set of coupled equations:

$$\dot{D}_q(t) = i\boldsymbol{\varepsilon}_0(t)\cdot\sum_p D_p(t)e^{-i(E_p-E_q)t}(\mathbf{M}_{qp}^{+}e^{-i\omega t} + \mathbf{M}_{qp}^{-}e^{i\omega t}). \tag{10}$$

The coupling between the excitonic eigenstates q and p and the spatiotemporally varying electric field is determined by the matrix elements $\mathbf{M}_{qp}^{\pm}$ which can be reduced to the transition dipole matrix elements of the individual clusters as

$$\mathbf{M}_{qp}^{\pm} = \sum_I e^{\pm i\mathbf{k}_\omega\cdot\mathbf{R}_I}\sum_{ij\ldots z}\sum_{k_I'} C_{ij\ldots k_I'\ldots z}^{*q}C_{ij\ldots k_I\ldots z}^{p}\boldsymbol{\mu}_{k_I'k_I}^{(I)}. \tag{11}$$

The solution of the set of equations (10) gives rise to the time-dependent coefficients $D_q(t)$ which allows for describing the time-dependent response of the whole cluster array. However, in order to simulate the spatial distribution of the electric field including the near-field zone, one needs to calculate the fields emitted by each individual component of the array. For this purpose, the total response needs to be partitioned into the contributions of the individual components, which we achieve by using the reduced density matrix formalism. The reduced

density operator for the Ith cluster is found as a partial trace of the full density operator over all other clusters

$$\hat{\rho}_I = \mathrm{Tr}_{1,\ldots,I-1,I+1,\ldots,N}(\hat{\rho}). \tag{12}$$

Assuming that the whole cluster array under consideration is in the pure state described by the wave function $|\Phi(t)\rangle$, the density operator can be written as

$$\hat{\rho} = |\Phi(t)\rangle\langle\Phi(t)|. \tag{13}$$

By employing the basis decomposition (9) for the reduced density operator (12), one obtains

$$\hat{\rho}_I = \sum_{pq} D_p(t) D_q^*(t) e^{-i(E_p - E_q)t} \times \sum_{ij\ldots z}\sum_{k_I'} C^{*q}_{ij\ldots k_I'\ldots z} C^{p}_{ij\ldots k_I\ldots z} \left|\Psi^{(I)}_{k_I}\right\rangle\left\langle\Psi^{(I)}_{k_I'}\right|. \tag{14}$$

The diagonal elements of the reduced density matrix in the basis $|\Psi^{(I)}_{k_I}\rangle$ provide the population of the corresponding electronic states of the selected cluster I, and the time-dependent dipole moment of the Ith cluster is determined according to

$$\begin{aligned}\mathbf{p}_I(t) &= \mathrm{Tr}(\hat{\boldsymbol{\mu}}_I \hat{\rho}_I) \\ &= \sum_{pq} D_p(t) D_q^*(t) e^{-i(E_p - E_q)t} \\ &\quad \times \sum_{ij\ldots z}\sum_{k_I'} C^{*q}_{ij\ldots k_I'\ldots z} C^{p}_{ij\ldots k_I\ldots z} \boldsymbol{\mu}^{(I)}_{k_I' k_I}.\end{aligned} \tag{15}$$

Finally, the electric field produced by each single cluster can be calculated using a dipole electromagnetic-field expression [48], and the total electric field distribution is obtained by summation over all subunits:

$$\begin{aligned}\mathbf{E}(\mathbf{r},t) = \sum_I^N \Bigg\{ \frac{-1}{r_I^3}\Bigg[&\mathbf{p}_I(t') + \frac{r_I}{c}\dot{\mathbf{p}}_I(t') \\ &- \frac{3\mathbf{r}_I}{r_I^2}\Bigg[\mathbf{r}_I \cdot \left(\mathbf{p}_I(t') + \frac{r_I}{c}\dot{\mathbf{p}}_I(t')\right)\Bigg] \\ &+ \frac{1}{c^2}\mathbf{r}_I \times (\ddot{\mathbf{p}}_I(t') \times \mathbf{r}_I)\Bigg]_{t'=t-\frac{r_I}{c}} \Bigg\},\end{aligned} \tag{16}$$

where $\mathbf{r}_I = \mathbf{r} - \mathbf{R}_I$ and r_I is its absolute value.

D. Construction of electronic Hamiltonian based on TDDFT

As already described in the previous sections, the essential quantities needed for the simulation of the response of a cluster array are the electronic Hamiltonians and the dipole coupling matrix elements of individual constituents. In principle, for molecular-sized clusters, these quantities can be obtained using any *ab initio* or semiempirical electronic-structure method. Due to its efficiency and applicability to relatively large complex systems, we have employed the linear response time-dependent density functional theory (TDDFT) in order to obtain the energies of the electronic states and the transition dipole moments between the ground and excited electronic states. In contrast to the ground-excited-state transition dipole moments, which can be calculated using standard TDDFT routines, the determination of the transition dipole matrix elements between different excited states requires approximate procedure presented in detail elsewhere [49]. Here, we only briefly outline the main steps involved.

Based on the Casida ansatz [50], the excited-state electronic wave function can be approximated by the configuration interaction singles-like expansion

$$|\Psi_k(\mathbf{r})\rangle = \sum_{i,a} c^k_{i,a} \left|\Phi^{\mathrm{CSF}}_{i,a}(\mathbf{r})\right\rangle, \tag{17}$$

where $|\Phi^{\mathrm{CSF}}_{i,a}(\mathbf{r})\rangle$ is a singlet spin-adapted configuration state function (CSF) defined as

$$\left|\Phi^{\mathrm{CSF}}_{i,a}(\mathbf{r})\right\rangle = \frac{1}{\sqrt{2}}\left(\left|\Phi^{a\beta}_{i\alpha}(\mathbf{r})\right\rangle + \left|\Phi^{a\alpha}_{i\beta}(\mathbf{r})\right\rangle\right), \tag{18}$$

and $|\Phi^{a\beta}_{i\alpha}(\mathbf{r})\rangle$ is a Slater determinant with two unpaired electrons, one on the occupied Kohn-Sham (KS) orbital i with spin α and another on the virtual orbital a with spin β. Correspondingly, in the determinant $|\Phi^{a\alpha}_{i\beta}(\mathbf{r})\rangle$, the unpaired electrons reside on the occupied KS orbital i (spin β) and the virtual orbital a (spin α). The expansion (17) gives rise to the wave functions for an arbitrary number of excited states of any symmetry and represents a practicable way of defining an excited-state wave function based on linear response TDDFT. Although these states do not correspond to the exact eigenstates of the molecular Hamiltonian and do not represent the variational approximation to them, they still can be used as an approximate basis to represent the molecular electronic eigenstates. In principle, once the approximate electronic wave function is available, all properties of the excited states such as dipole couplings can be straightforwardly calculated.

The expansion coefficients $c^k_{i,a}$ in Eq. (17) are determined on physical grounds by requiring that the wave function in Eq. (17) leads to the same density response as the one obtained by the linear response TDDFT procedure. Thus, for nonhybrid functionals without exact exchange the coefficients $c^k_{i,a}$ are given by

$$c^k_{i,a} = (\epsilon_a - \epsilon_i)^{-1/2}\left(X^k_{ia} + Y^k_{ia}\right), \tag{19}$$

where ϵ_i and ϵ_a are the orbital energies of ith occupied and ath virtual single-electron orbitals, respectively, and X^k and Y^k represent the solution of the TDDFT eigenvalue problem [50,51]. This allows us to define the set of mutually orthogonal electronic wave functions $|\Psi_k(\mathbf{r})\rangle$ which is further employed to calculate the transition dipole matrix elements $\boldsymbol{\mu}_{k'k}$ between the electronic states of the cluster as

$$\begin{aligned}\boldsymbol{\mu}_{k'k} &= \langle\Psi_{k'}(\mathbf{r})|\hat{\boldsymbol{\mu}}|\Psi_k(\mathbf{r})\rangle \\ &= \sum_{ia}\sum_{i'a'} \left(c^{k'}_{i',a'}\right)^* c^k_{i,a} \left\langle\Phi^{\mathrm{CSF}}_{i',a'}(\mathbf{r})\right|\hat{\boldsymbol{\mu}}\left|\Phi^{\mathrm{CSF}}_{i,a}(\mathbf{r})\right\rangle,\end{aligned} \tag{20}$$

where a and a' indicate virtual and i and i' occupied orbitals, respectively. The dipole matrix elements between the CSF's on the right-hand side of Eq. (20) can be reduced to the transition dipole moments between Kohn-Sham orbitals [49,52], which can be calculated using the standard quantum-chemical integration routines.

E. Approximate iterative approach for the simulation of electromagnetic field propagation

While the solution of the Eqs. (10) and (16) describes the coupled evolution of the system and the electromagnetic fields completely, in practice it can not be applied to a wide range of systems of interest. The solution quickly becomes cumbersome if a large number of electronic states per constituent and large number of constituents are considered. Since the inclusion of many electronic states in the simulation is mandatory for the description of the nonlinear response of clusters, the straightforward solution of Eqs. (10) and (16) is restricted to relatively small arrays only. Thus, in order to be able to treat the electric field propagation in larger systems, we introduce an approximate iterative procedure for the simulation of electromagnetic response of the system and the electric field evolution. In this approach, we solve the TDSE for each subunit independently:

$$i\frac{\partial}{\partial t}|\Phi_I(t)\rangle = \hat{\mathrm{H}}_I|\Phi_I(t)\rangle, \tag{21}$$

with the Hamiltonian $\hat{\mathrm{H}}_I$ determined according to (1). The single-cluster wave function $|\Phi_I(t)\rangle$ is expanded in the basis spanned by the eigenfunctions of the field-free single-cluster Hamiltonian $\hat{\mathrm{H}}_0^{(I)}$:

$$|\Phi_I(t)\rangle = \sum_i C_i^{(I)}(t)e^{-iE_i^{(I)}t}\left|\Psi_i^{(I)}\right\rangle. \tag{22}$$

Due to the same reasons as discussed in Sec. II C, the external electric field vector can be written as $\boldsymbol{\varepsilon}_{\mathrm{ext}}(\mathbf{r},t) \approx \boldsymbol{\varepsilon}_0(t)(e^{i(\mathbf{k}_\omega\cdot\mathbf{r}-\omega t)} + \text{c.c.})$. With this assumption, the TDSE (21) is transformed in a set of differential equations for the time-dependent expansion coefficients $C_i^{(I)}(t)$:

$$\begin{aligned}\dot{C}_i^{(I)}(t) = {} & i\boldsymbol{\varepsilon}_{\mathrm{ext}}(\mathbf{R}_I,t)\sum_j C_j^{(I)}(t)e^{-i(E_j^{(I)}-E_i^{(I)})t}\boldsymbol{\mu}_{ij}^{(I)} \\ & + i\sum_j C_j^{(I)}(t)e^{-i(E_j^{(I)}-E_i^{(I)})t} \\ & \times \sum_{J\neq I}\left\langle\Psi_i^{(I)}\left|\hat{\boldsymbol{\mu}}_I\cdot\boldsymbol{\varepsilon}_J(\mathbf{r},t)\right|\Psi_j^{(I)}\right\rangle.\end{aligned} \tag{23}$$

Considering the fact that the overlap between the electronic wave functions $|\Psi_i^{(I)}\rangle$ and $|\Psi_j^{(I)}\rangle$ is nonzero only in the space close to the cluster, the matrix element on the right-hand side of Eq. (23) can be simplified as $\langle\Psi_i^{(I)}|\hat{\boldsymbol{\mu}}_I\cdot\boldsymbol{\varepsilon}_J(\mathbf{r},t)|\Psi_j^{(I)}\rangle \approx \boldsymbol{\varepsilon}_J(\mathbf{R}_I,t)\boldsymbol{\mu}_{ij}^{(I)}$. The electric field $\boldsymbol{\varepsilon}_J(\mathbf{R}_I,t)$ produced by the Jth cluster is determined via the time-dependent dipole moment of that cluster [48]

$$\begin{aligned}\boldsymbol{\varepsilon}_J(\mathbf{R}_I,t) = {} & \frac{-1}{r_{IJ}^3}\Bigg[\mathbf{p}_J(t') + \frac{r_{IJ}}{c}\dot{\mathbf{p}}_J(t') \\ & - \frac{3\mathbf{r}_{IJ}}{r_{IJ}^2}\left[\mathbf{r}_{IJ}\cdot\left(\mathbf{p}_J(t') + \frac{r_{IJ}}{c}\dot{\mathbf{p}}_J(t')\right)\right] \\ & + \frac{1}{c^2}\mathbf{r}_{IJ}\times(\ddot{\mathbf{p}}_J(t')\times\mathbf{r}_{IJ})\Bigg]_{t'=t-\frac{r_{IJ}}{c}},\end{aligned} \tag{24}$$

while the time-dependent dipole moment itself is calculated as the expectation value of the respective dipole moment operator:

$$\begin{aligned}\mathbf{p}_J(t) &= \langle\Phi_J(t)|\hat{\boldsymbol{\mu}}_J|\Phi_J(t)\rangle \\ &= \sum_{ij} C_i^{*(J)}(t)C_j^{(J)}(t)e^{-i(E_j^{(J)}-E_i^{(J)})t}\boldsymbol{\mu}_{ij}^{(J)}.\end{aligned} \tag{25}$$

Here, $C_j^{(J)}(t)$ are the expansion coefficients determined by solving the set of equations (23). The time-dependent dipole moments $\mathbf{p}_J(t)$ are then employed to calculate the electric fields of the individual subunits which will act on all other constituents of the array. Since the response of each subunit is dependent on all the others, an iterative, "self-consistent" procedure is needed in order to simulate the evolution of the system and the electromagnetic field.

Consequently, we proceed as follows: (i) The set of Eqs. (23) is solved with the cluster-response electric fields set to zero [$\boldsymbol{\varepsilon}_J(\mathbf{R}_I,t) = 0$] and the first approximation to the time-dependent expansion coefficients $C_k^{0(I)}(t)$ is obtained. (ii) The time-dependent dipole moments $\mathbf{p}_J^0(t)$ of all clusters in the array are calculated by means of Eq. (25). (iii) The response of all clusters is determined by calculating $\boldsymbol{\varepsilon}_J^0(\mathbf{R}_I,t)$ via Eq. (24) and used in the set of Eqs. (23) to find the next approximation to the expansion coefficients $C_k^{1(I)}(t)$.

Steps (ii) and (iii) are repeated until the time-dependent dipole moments, obtained in subsequent iterations, do not change within a certain threshold:

$$\delta = \frac{1}{T}\sum_J\int_0^T\left|\mathbf{p}_J^{i+1}(t) - \mathbf{p}_J^i(t)\right|dt < \epsilon, \tag{26}$$

where T is the simulation time. The convergence of the method is ensured by the fact that the main contribution to the total electric field comes from the external laser radiation, and the cluster-induced fields are smaller compared to the external one. Finally, the electric field vector is calculated according to Eq. (16) with time-dependent dipole moments determined by means of Eq. (25) using the expansion coefficients found in the last iteration.

III. COMPUTATION DETAILS

In the present contribution, the above-described methods for the simulation of the optical response of metal-cluster arrays are applied to pairs of identical Ag_2 or Ag_8 clusters as well as to a triangular array consisting of six identical Ag_8 clusters. The simulation proceeded as follows: First, for each type of silver clusters, the equilibrium structure has been determined by the full geometry optimization in the ground electronic state employing DFT with the gradient-corrected Becke-Lee-Yang-Parr (BLYP) exchange-correlation functional [53,54], combined with the triple-zeta valence plus polarization Gaussian atomic basis set (TZVP) [55] and a relativistic 19-electron effective core potential for silver [56]. Subsequently, a number of excited-electronic-state energies $E_i^{(I)}$ has been calculated employing linear response TDDFT. All calculations have been performed using the TURBOMOLE V.6.3 package [57,58]. The number of excited states taken into consideration was 10 for Ag_2 and 40 for Ag_8, covering the energy range up to 4.5 and 4.1 eV, respectively. Then, the

transition dipole moments $\boldsymbol{\mu}_{ij}^{(I)}$ between all the states were determined according to Eq. (20).

Subsequently, for the cluster pairs, the Hamiltonian (5) has been constructed and diagonalized. Based on the eigenvalues and eigenvectors of the Hamiltonian (5), the absorption spectra of the cluster pairs were calculated. To check the accuracy of the excitonic model, the resulting spectra for Ag_2 cluster pairs at $10a_0$ and $20a_0$ separation have been compared with more accurate CC2 calculations [59,60]. The CC2 model is an approximation to the coupled cluster singles and doubles model and provides excitation energies correct to the second order and transition moments correct to the first order [47] at reasonable computation time.

To simulate the optical response of the cluster pairs, the TDSE (10) was integrated using the fourth-order Runge-Kutta method with a time step of 1×10^{-4} fs. For the Ag_2 cluster pair, the integration was performed within all the 121 eigenstates obtained after diagonalization of the Hamiltonian, while for the Ag_8 cluster pair only the 450 lowest eigenstates were taken into account. Along the TDSE integration, the time-dependent dipole moments of each cluster in the pair were calculated according to Eq. (15) with a time step of 2×10^{-3} fs.

For comparison, the optical response of the Ag_2 and Ag_8 cluster pairs has been also simulated using the approximate iterative approach presented in Sec. II E. The TDSE (23) was integrated for each cluster within the manifold of 10 electronic excited states for Ag_2 and 40 for Ag_8, with the same time step of 1×10^{-4} fs.

Finally, the simulation of light propagation in the Ag_8 cluster triangle constructed of six subunits was performed employing the iterative method described in Sec. II E. The TDSE (23) was propagated within 40 electronic excited states for 100 fs. The integration time step was 1×10^{-4} fs, the number of iterations required for convergence was 37. Afterwards, the electric field vector was calculated according to Eq. (16) on a three-dimensional (3D) spatial grid with a step of $0.35a_0$.

IV. RESULTS AND DISCUSSION

A. *Ab initio* excitonic Hamiltonians and optical properties of Ag_2 and Ag_8 cluster pairs

In this section, we investigate first the optical properties of Ag_2 and Ag_8 cluster pairs based on the external field-free excitonic Hamiltonians $\hat{H}_{arr}$ obtained from *ab initio* TDDFT calculations. The first system we present is a dimer of two identical Ag_2 subunits placed at a distance r_{12} and oriented such that the transition dipole moments for the first intense transition $S_0 \rightarrow S_1$ are collinear to each other and both perpendicular to the vector $\mathbf{r}_{12}$ connecting the clusters' charge centers, as shown in the inset of Fig. 1(a). The electronic states of the Ag_2 cluster pair obtained by the diagonalization of the excitonic Hamiltonian [Eq. (5)] are presented in Fig. 1(a) as functions of the intercluster distance and compared to the energies of the pair at infinite separation. As can be seen, the energies of the eigenstates converge relatively fast to the asymptotic limit such that at distances larger than $20a_0$, effectively no excitonic coupling is present.

The pair of Ag_8 clusters is oriented analogously to the Ag_2 such that the transition dipoles for the lowest intense transition $S_0 \rightarrow S_{10}$ are parallel to each other and both perpendicular to the vector $\mathbf{r}_{12}$ which connects the charge centers of the clusters [see inset in Fig. 1(b)]. The cluster-pair excitonic eigenstates are displayed in Fig. 1(b) together with their infinite

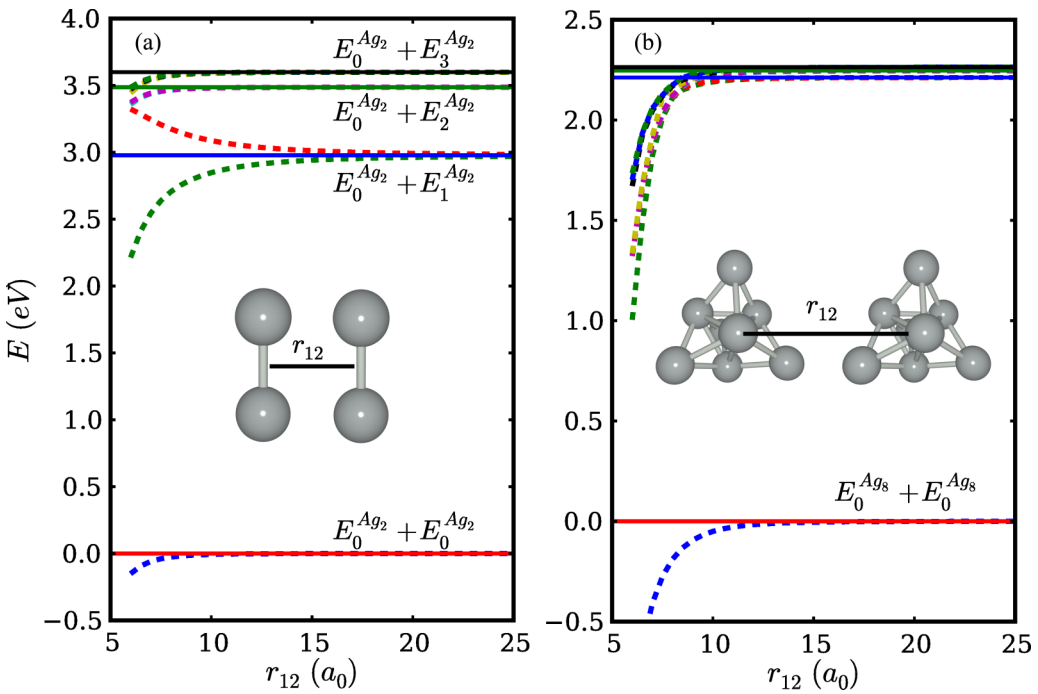

FIG. 1. (Color online) (a) The nine lowest eigenvalues of the Hamiltonian (5) of Ag_2 cluster pair (dashed lines) as functions of the intercluster distance r_{12}; (solid lines) the combinations of single Ag_2 cluster energies $E_i^{Ag_2} + E_j^{Ag_2}$. (b) The same as in (a) but for Ag_8 clusters. The solid lines correspond to (from bottom to top) $E_0^{Ag_8} + E_0^{Ag_8}$, $E_0^{Ag_8} + E_1^{Ag_8}$, $E_0^{Ag_8} + E_2^{Ag_8}$, and $E_0^{Ag_8} + E_3^{Ag_8}$ single Ag_8 cluster energies.

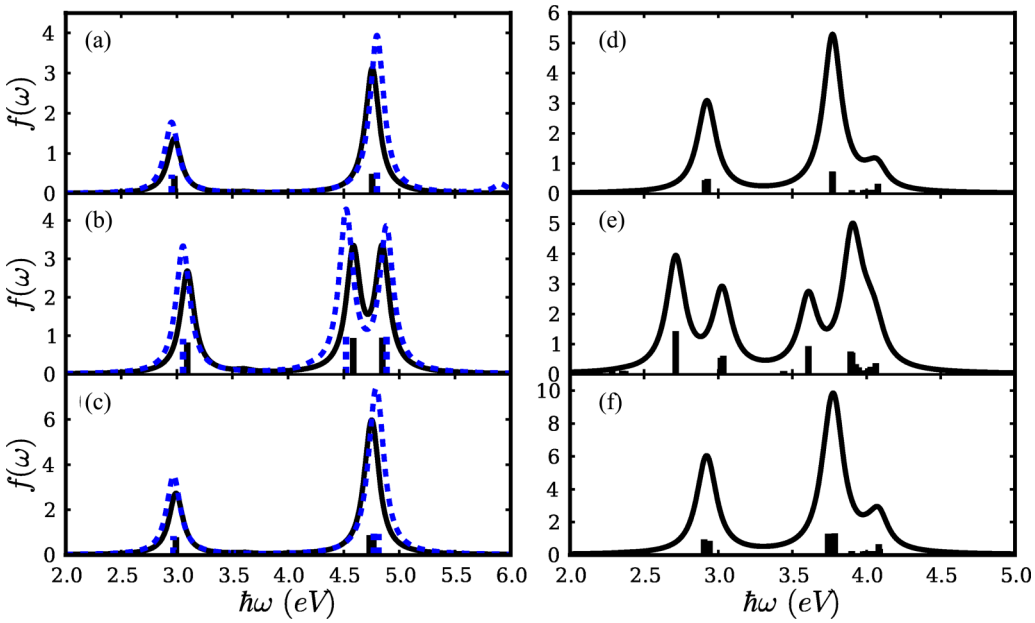

FIG. 2. (Color online) (Left panel) Absorption spectra of (a) a single Ag_2 cluster, (b) a pair of Ag_2 clusters placed at $10a_0$ distance, and (c) a pair of Ag_2 clusters at $20a_0$ separation. Solid lines represent the results of calculations based on excitonic Hamiltonian (3) and dashed lines represent the results of *ab initio* CC2 calculations. (Right panel) Absorption spectra of (d) single Ag_8 cluster, of a pair of Ag_8 clusters at (e) $10a_0$ and (f) $20a_0$ separation calculated based on excitonic Hamiltonian (3). All the spectra are folded with Lorentzian shape functions with full width at half maximum (FWHM) equal to 0.3 eV.

separation limit. For the Ag_8 pair, the excitonic eigenvalues converge to the sums of single Ag_8 cluster energies already at an intercluster distance of $13a_0$.

The electronic absorption spectra of the Ag_2 and Ag_8 cluster pairs calculated using the excitonic eigenfunctions for the $10a_0$ and $20a_0$ separation are presented in Fig. 2 and compared with the absorption spectra of the individual clusters. Additionally, for Ag_2 the results of more accurate *ab initio* correlated CC2 calculations are shown with dashed lines. As it can be seen, at $20a_0$ separation the electronic absorption spectrum corresponds in both cases closely to the spectrum of the individual subunit and the exciton splitting of the electronic states is negligible [compare Figs. 2(a) and 2(c) for Ag_2 and Figs. 2(d) and 2(f) for Ag_8]. When the distance between the clusters is reduced, the spectrum of the pair is changed dramatically. In the case of the Ag_2 pair, the low-energy absorption band is 0.1 eV blue-shifted due to repulsive character of the corresponding excited state $|\psi_2\rangle$ [cf. Figs. 1(a) and 2(b)] which arises due to the parallel orientation of the dipole moments. The lower-lying $|\psi_1\rangle$ state has attractive character, but due to the *gerade* symmetry does not have any intensity. The higher absorption band in the energy range between 4.5 and 5.0 eV is split due to the exciton coupling with a splitting of ∼0.3 eV at $10a_0$ distance. The results of more accurate CC2 calculations fully support these findings. Namely, the blue-shift of the lower absorption band is 0.09 eV and the splitting of the higher absorption band is 0.4 eV at $10a_0$ separation. The electronic absorption spectrum of the Ag_8 cluster pair is presented in Figs. 2(d)–2(f). The spectrum exhibits splittings both in low- as well as in high-energy regions at $10a_0$ separation, while for larger distances between silver clusters it closely resembles the single-cluster absorption spectrum.

B. Laser-driven exciton dynamics in the Ag_2 cluster pair

In order to validate the approximate iterative approach for the simulation of the optical response of cluster arrays introduced in Sec. II E, we compare it with the full quantum-mechanical approach presented in Sec. II A. The exciton dynamics of the Ag_2 cluster pair has been induced by an external laser pulse with the temporal profile described by the Gaussian function

$$\boldsymbol{\varepsilon}_0(t) = \frac{1}{2}\varepsilon_{\max} \exp\left(-\frac{(t-t_0)^2}{2\sigma^2}\right), \tag{27}$$

with the full width at half maximum (FWHM) of 27 fs (σ = 11.5 fs) corresponding to the spectral FWHM of 0.14 eV. The central frequency of the pulse $\omega_c = 2.98$ eV is resonant to the intense $S_0 \rightarrow S_1$ transition of a single Ag_2 cluster. The peak pulse strength is $\varepsilon_{\max} = 5 \times 10^{-3}\, E_h/ea_0$, and the pulse is centered at $t_0 = 30$ fs. The field propagates along the vector pointing from the center of the first cluster to that of the second one (x axis in the following) and is polarized along the $S_0 \rightarrow S_1$ transition dipole moment (y axis).

First, we investigate the population dynamics in the Ag_2 cluster pair with intercluster separation of $10a_0$. Since at this separation the intense transition is blue-shifted (cf. Fig. 2), the external pulse is not resonant to it, although the frequency of the transition still lies within the spectral FWHM of the pulse. The excitonic state population dynamics of the cluster pair at $10a_0$ separation is presented in Fig. 3(a). The excitonic eigenstates together with the excitation energies and projections of the transition dipole moments on the pulse polarization direction between the states involved in the dynamics are presented in Fig. 3(b). As it can be seen from the figure, at first the laser pulse causes the exciton-state

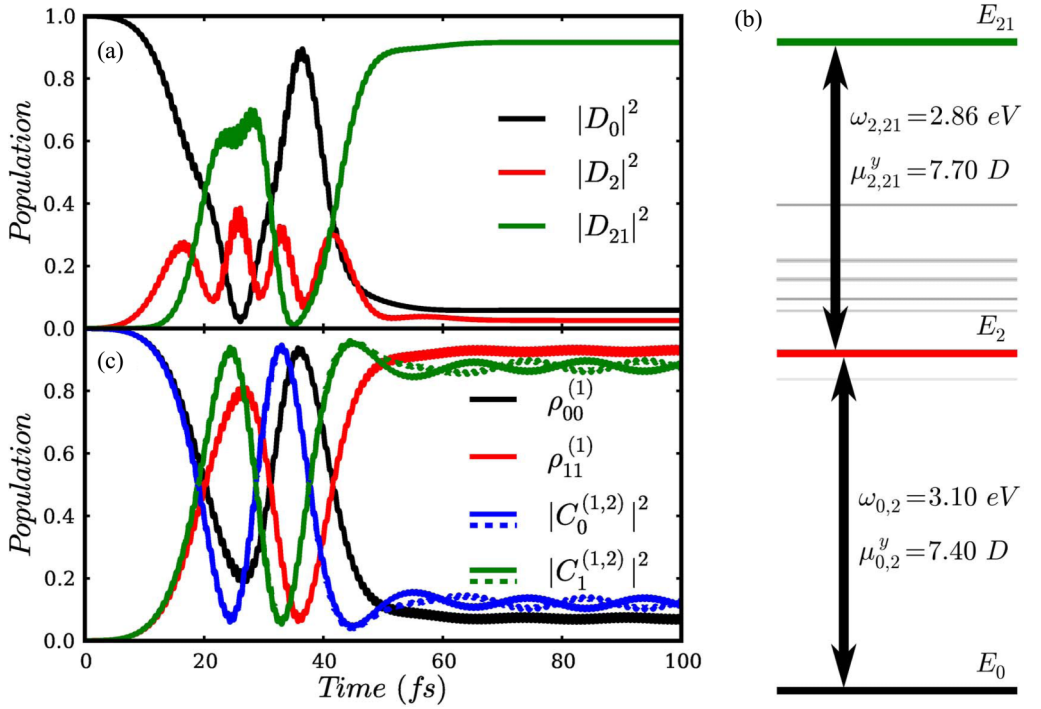

FIG. 3. (Color online) (a) Population dynamics of the Ag_2 cluster pair with $10a_0$ spacing. The coefficients D_i are the solutions of Eq. (10) and thus $|D_i|^2$ represent the population of the corresponding eigenstate of the Hamiltonian $\hat{H}_{arr}$. (b) Energy-level structure of the Ag_2 cluster pair together with the excitation energies and projections of the transition dipole moments on the laser field polarization direction. (c) Population dynamics of single clusters in the Ag_2 cluster pair. $\rho_{00}^{(1)}$ and $\rho_{11}^{(1)}$ are the diagonal elements of the reduced density matrix (14) of the first cluster in the pair, which describe the population of the ground and first excited states of the cluster, respectively. $C_0^{(1)}$ and $C_1^{(1)}$ are the coefficients in the expansion (22) for the first cluster, $C_0^{(2)}$ and $C_1^{(2)}$ the coefficients for the second cluster (shown with dashed lines of the same color) obtained using iterative approach.

population transfer to the $|\psi_2\rangle$ state, which corresponds to excitation of one of the clusters in the pair, since in the basis (4) this eigenfunction reads as

$$|\psi_2\rangle \approx \frac{1}{\sqrt{2}}\left(\left|\Psi_0^{(1)}\right\rangle \otimes \left|\Psi_1^{(2)}\right\rangle + \left|\Psi_1^{(1)}\right\rangle \otimes \left|\Psi_0^{(2)}\right\rangle\right). \quad (28)$$

Further, the population is transferred to the $|\psi_{21}\rangle$ state since the transition $|\psi_2\rangle \rightarrow |\psi_{21}\rangle$ also lies within the FWHM of the laser pulse. The state $|\psi_{21}\rangle$ corresponds to the simultaneous excitation of both clusters since the main contribution to this eigenstate comes from the $|\Psi_1^{(1)}\rangle \otimes |\Psi_1^{(2)}\rangle$ basis function. Afterwards, the population is cycled back to the ground state through the same intermediate state. Overall, the system performs approximately 1.5 cycles of oscillations before the laser pulse ceases.

Finally, from the total cluster-system wave function, the elements of reduced density matrices of both clusters are calculated according to Eq. (14). The diagonal elements of the reduced density matrices $\rho_{ii}^{(I)}$ describe the population dynamics of a single cluster, which we compare to the population dynamics calculated via the iterative approach described in Sec. II E. The results of both calculations are presented in Fig. 3(c). It can be seen that the iterative approach predicts a slightly shorter period of population oscillations between ground and first excited states of a single cluster, although qualitatively the population dynamics is represented correctly. While the external laser pulse acts, the results for both clusters are essentially the same, but after the external pulse ceases the population of the selected states of the first and second cluster starts to oscillate out of phase, showing the excitation transfer between these clusters. These oscillations are clearly seen in the population dynamics calculated via iterative approach [cf. Fig. 3(c), $|C_i^{(1)}|^2$ and $|C_i^{(2)}|^2$], but are present, though difficult to show on the same plot, in reduced density matrix elements dynamics as well. Therefore, only diagonal elements for the first cluster $\rho_{ii}^{(1)}$ are presented in Fig. 3(c).

The population dynamics of the Ag_2 cluster pair at $20a_0$ separation under the same external laser pulse action was investigated in a similar manner, and the results are presented in Fig. 4. At this intercluster separation, the spectrum of the cluster pair is almost unchanged compared to the single Ag_2 cluster spectrum and thus the laser pulse is resonant to the intense $|\psi_0\rangle \rightarrow |\psi_2\rangle$ and $|\psi_2\rangle \rightarrow |\psi_{21}\rangle$ transitions, as is seen in Fig. 4(b). During the pulse action, the system exhibits almost two cycles of Rabi-type oscillations between the $|\psi_0\rangle$ and $|\psi_{21}\rangle$ states including the intermediate $|\psi_2\rangle$ state [cf. Fig. 4(a)]. As in the previous case, $|\psi_0\rangle$ corresponds to the stationary state with both clusters in the ground state, $|\psi_2\rangle$ is the combination (28), and $|\psi_{21}\rangle$ is the stationary state with two clusters promoted to the first excited state.

The population dynamics of the first cluster in the pair is shown in Fig. 4(c). The diagonal elements of reduced density matrix $\rho_{00}^{(1)}$ and $\rho_{11}^{(1)}$, retrieved from quantum-mechanical calculations, are compared to the state populations $|C_0^{(1)}|^2$ and $|C_1^{(1)}|^2$, obtained by the iterative method. It is seen that

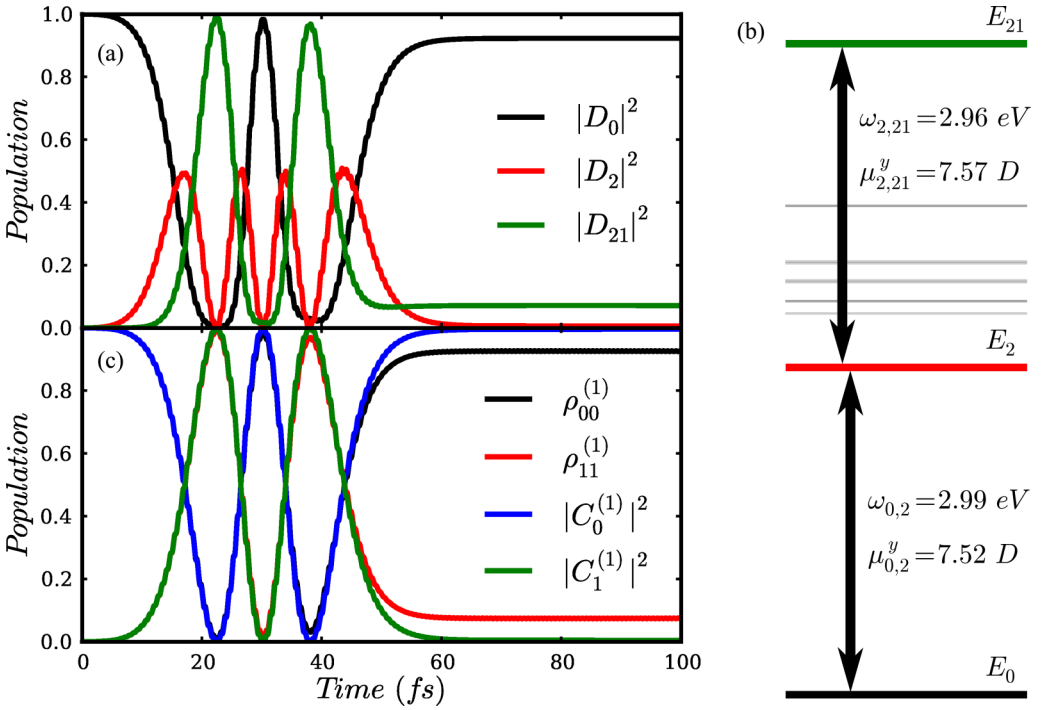

FIG. 4. (Color online) (a) Population dynamics of the Ag_2 cluster pair with $20a_0$ spacing, (b) energy-level structure of the Ag_2 cluster pair together with the excitation energies and projections of the transition dipole moments on the laser field polarization direction, (c) population dynamics of the first cluster in the cluster pair.

at $20a_0$ intercluster separation the iterative approach almost perfectly reproduces the results of fully quantum-mechanical calculations. The period of Rabi oscillations is the same for both methods, and the final populations of the ground and first excited states differ only by 0.07. The results for the second cluster are essentially the same and thus not presented.

In the following, we compare the dipole moments of a single cluster in the pair at both intercluster separations by employing the two theoretical approaches described in Secs. II A and II E. In Fig. 5, we present the y component of the dipole moment vector of the first cluster in the pair calculated by means of Eq. (15) (shown with thick black line) and Eq. (25) [thin red (gray) line]. The other components of the dipole moment vector are negligibly small. As expected, at $10a_0$ separation the results of the two approaches differ considerably as it is seen in Fig. 5(a), while at $20a_0$ intercluster distance the results closely match [cf. Fig. 5(b)].

Finally, we investigate the convergence of the iterative approach for the two systems discussed above. In Fig. 6, the deviation δ [as defined in Eq. (26)] is plotted versus the number of iteration. It is seen that at $10a_0$ separation the iterative approach requires approximately 50 iterations to converge, while at $20a_0$ separation only 20 iterations are needed.

The analysis of the population dynamics and time-dependent dipole moments allows us to conclude that, at intercluster separations at which the system absorption spectrum is close to the absorption spectrum of a single cluster [cf. Figs. 2(a)–2(c)], the iterative approach described in Sec. II E can be used to efficiently model the response of ordered cluster arrays to the external electric field.

C. Exciton dynamics in the Ag_8 cluster pair

In this section, we investigate laser-driven exciton dynamics in a more complicated system, namely, an Ag_8 cluster pair placed at $20a_0$ distance. The results for the Ag_2 cluster pair have demonstrated that at this distance the iterative approach closely resembles the results of full quantum-mechanical

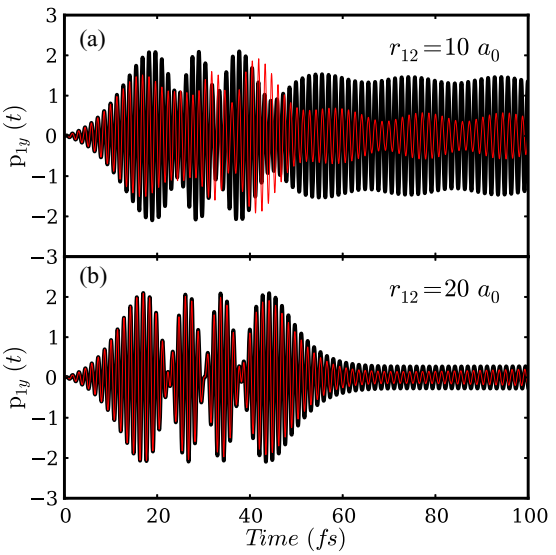

FIG. 5. (Color online) Time-dependent dipole moment of the first cluster of the Ag_2 cluster pair with the components placed at (a) $10a_0$ separation, (b) $20a_0$ separation. The results obtained by solving Eq. (15) are shown with thick black lines and via iterative approach [Eq. (25)] with thin red (gray) lines.

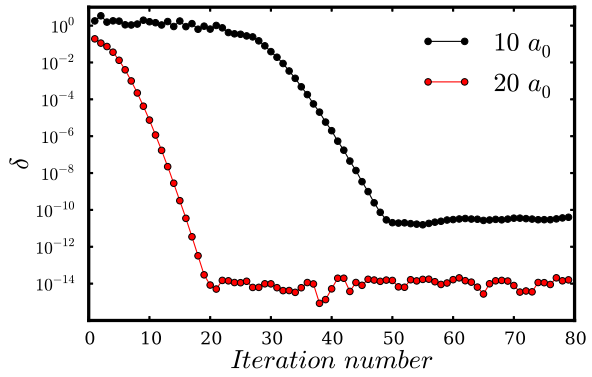

FIG. 6. (Color online) Dependence of the difference between single-cluster dipole moments obtained in subsequent iterations δ on the iteration number for Ag_2 cluster systems with intercluster separation of $10a_0$ and $20a_0$.

calculations. In a simulation, population dynamics is initiated by a laser pulse of the same temporal profile as for the Ag_2 system [see Eq. (27)], with the central frequency $\omega_c = 2.91$ eV being resonant to the intense $S_0 \rightarrow S_{10}$ transition in isolated Ag_8. The polarization of the external laser pulse is aligned with the direction of the $S_0 \rightarrow S_{10}$ transition dipole moment vector.

Similarly to the case of the Ag_2 cluster pair, under the laser pulse action the population is transferred from the ground state $|\psi_0\rangle$ to the resonant excited state $|\psi_{22}\rangle$ [cf. Fig. 7(a)]:

$$|\psi_{22}\rangle \approx 0.707\left(\left|\Psi_0^{(1)}\right\rangle \otimes \left|\Psi_{10}^{(2)}\right\rangle + \left|\Psi_{10}^{(1)}\right\rangle \otimes \left|\Psi_0^{(2)}\right\rangle\right) - 0.01\left(\left|\Psi_0^{(1)}\right\rangle \otimes \left|\Psi_{16}^{(2)}\right\rangle + \left|\Psi_{16}^{(1)}\right\rangle \otimes \left|\Psi_0^{(2)}\right\rangle\right), \quad (29)$$

which involves not only the ground (S_0) and resonant excited (S_{10}) states of each cluster, but also has a small contribution of the excited state S_{16}. Although the latter state is not resonant to the external laser pulse (the corresponding excitation energy is 3.77 eV), the oscillator strength of this transition is about two times higher than that for the $S_0 \rightarrow S_{10}$ transition, and the transition dipole moment is aligned with the polarization of the laser pulse as well. From the excited state $|\psi_{22}\rangle$, the population is further promoted to the higher excited state $|\psi_{266}\rangle$, which is mainly composed of the $|\Psi_{10}^{(1)}\rangle \otimes |\Psi_{10}^{(2)}\rangle$ basis function. As it is seen in Fig. 7(b), the transition $|\psi_{22}\rangle \rightarrow |\psi_{266}\rangle$ is also resonant to the exciting laser pulse, and the transition dipole moment has significant magnitude and is aligned along the polarization of the pulse. In this manner, the cluster pair performs 1.5 cycles of Rabi-type oscillations until the external pulse ceases.

The population dynamics of the first cluster in the pair calculated via iterative method is shown in Fig. 7(c) in comparison with the results retrieved from the full quantum-mechanical calculations. The results for the second cluster are essentially the same and thus not presented. The period of Rabi oscillations between the ground and resonant excited states is the same in both simulations, the difference between the final populations of the states of interest differ only by 0.07. Similarly to the Ag_2 cluster pair at $20a_0$ separation, the time-dependent dipole moments of each Ag_8 cluster in the pair calculated by both described methods [i.e., Eqs. (15) and (25)] demonstrate good agreement. The convergence of the iterative approach was reached within 16 iterations.

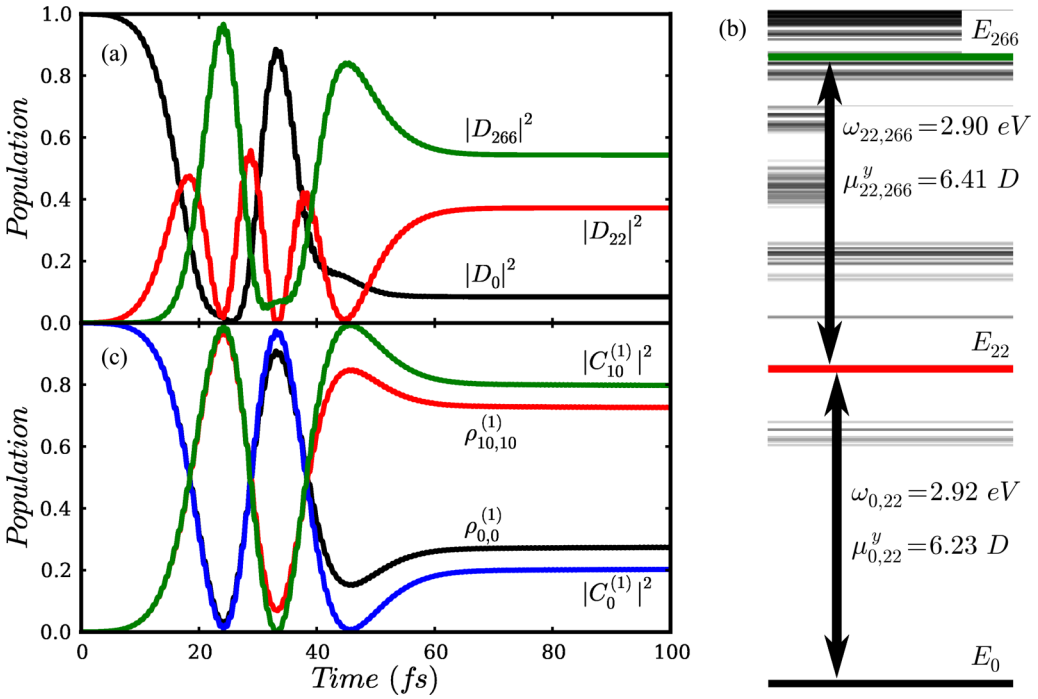

FIG. 7. (Color online) (a) Population dynamics of the Ag_8 cluster pair with $20a_0$ spacing. (b) Energy-level structure of the Ag_8 cluster pair together with the excitation energies and projections of the transition dipole moments on the direction of the laser field polarization. (c) Population dynamics of the first Ag_8 cluster in the pair. $\rho_{00}^{(1)}$ and $\rho_{10,10}^{(1)}$ are the diagonal elements of the reduced density matrix (14), $C_0^{(1)}$ and $C_{10}^{(1)}$ are the coefficients in the expansion (22).

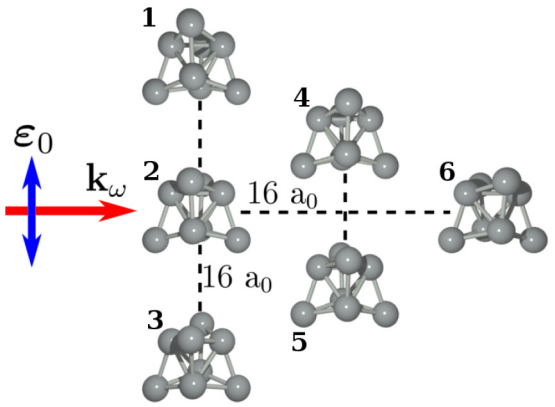

FIG. 8. (Color online) Schematic representation of the Ag_8 cluster array under the external laser pulse action. The distance between centers of neighboring subunits in each column is $16a_0$ and the same distance is between central lines of neighboring columns. Vector $\mathbf{k}_\omega$ shows the direction of the laser field propagation and vector $\boldsymbol{\varepsilon}$ denotes the direction of light polarization.

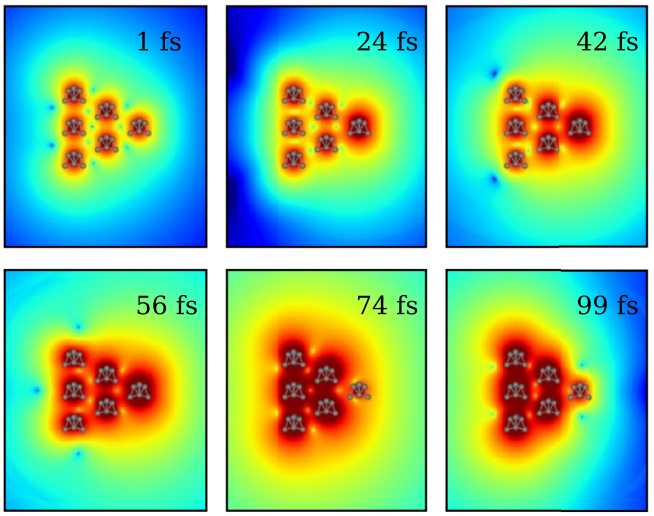

FIG. 10. (Color online) Spatial distribution of the electric field produced by a Ag_8 cluster array of triangular shape. The snapshots are taken in the plane of the array at different instants of time specified on the snapshots. The intensity of the electric field is denoted with a color code.

D. Simulation of light propagation in an Ag_8 cluster triangle

Finally, we apply our iterative approach in order to simulate the spatial distribution of the time-dependent electric field generated by a triangle built of Ag_8 clusters with a geometry as shown in Fig. 8. For the excitation we employ the same laser pulse as in the case of the Ag_8 cluster pair presented in Sec. IV C. The directions of the laser pulse propagation and polarization are shown in Fig. 8, the silver clusters are oriented in such a way that the transition dipole moment of the resonant $S_0 \rightarrow S_{10}$ transition is parallel to the field polarization.

During the pump-pulse action (0–50 fs of the simulation time), the population dynamics of each single cluster in the array is approximately the same (see Fig. 9). All silver clusters perform 1.5 cycles of Rabi oscillations between the ground and the resonant S_{10} excited states and the effect of cluster-cluster interactions is almost not seen. After the pump pulse has ceased, the population dynamics of unsymmetrically placed clusters becomes substantially different. The excited S_{10} state population of the "tip" cluster (numbered 6 in Fig. 8) decreases transferring the excitation energy to the neighboring clusters (4 and 5 in Fig. 8) which not only slows the population decay from the S_{10} excited state, but also promotes electron population to the close-lying S_{11} and S_{12} excited states. Although these

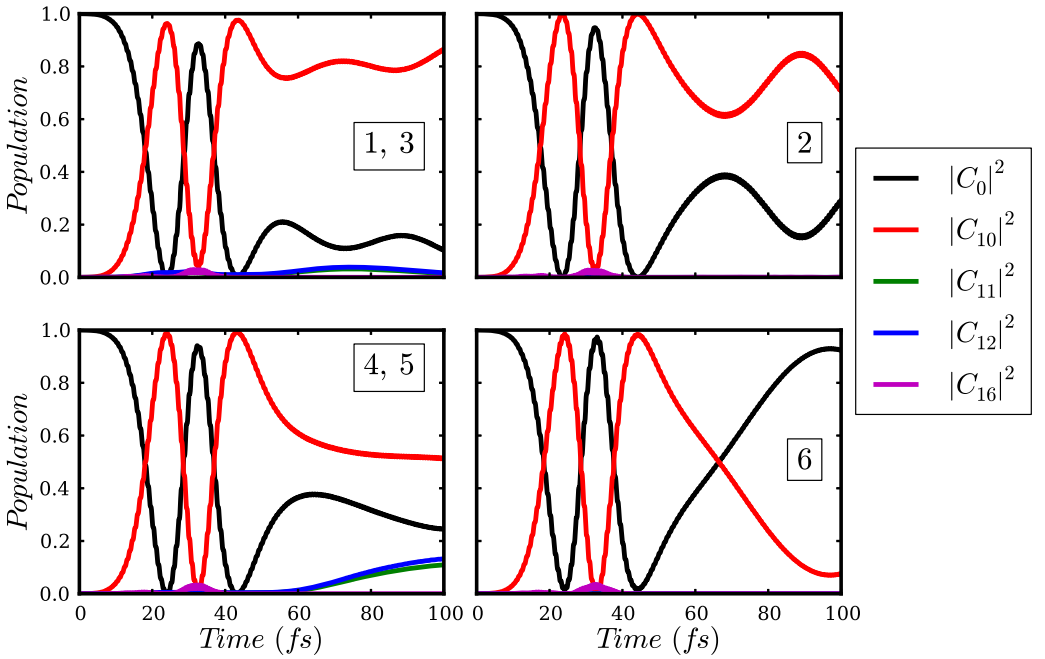

FIG. 9. (Color online) Population dynamics of each single cluster in the Ag_8 array calculated according to Eq. (23). Numbers on subplots correspond to cluster numbering in Fig. 8.

states have excitation energies within the spectral FWHM of the external laser pulse, they were not populated directly by the laser pulse due to the transition dipole moments perpendicular to the external field polarization. Small population of the S_{11} and S_{12} excited states is observed for other off-axis clusters (1 and 3).

The spatial variation of the electric field intensity in the plane of the silver cluster array at different times is presented in Fig. 10. The simulations show that, while the external pulse acts the intensity of the electric field around the cluster six increases, demonstrating not only excitation by the external laser pulse, but also excitation transfer from other clusters in the array. After the pulse ceases, the excitation is transferred back to the left part of the array as it is confirmed by the population dynamics. In general, the electric field of the cluster system shows rapid variation with time, and highly inhomogeneous spatial distribution, illustrating the possibility to coherently control the light propagation in such ordered arrays of molecular-sized silver clusters and to localize it spatially at selected times.

V. CONCLUSION

In conclusion, we have introduced two methods for the simulation of the light propagation in molecular-size cluster arrays. The first method is based on numerical integration of the TDSE with an excitonic Hamiltonian constructed based on *ab initio* TDDFT calculations under the influence of the external electric field. The reduced density matrix formalism is used to partition the array dipole response into contributions of the individual clusters. Subsequently, classical electrodynamics methods are used to determine the spatiotemporal distribution of the electric field produced by the whole array.

The second method represents an iterative approximation to the first one and is suitable for extended arrays. Instead of constructing the excitonic Hamiltonian of the whole array, for each subunit the TDSE is propagated separately under the action of the external laser field and the electric fields produced by the other clusters in the array. Time-dependent dipole moments obtained in a self-consistent manner are used to simulate the electric field of the array analogously to the first method.

Both methods were tested first on the Ag_2 cluster pair, and it was demonstrated that at relatively large intercluster separation, the iterative approach successfully reproduces the results of the excitonic Hamiltonian method. The approach is also valid when applied to systems with more complicated electronic structure, namely, Ag_8 clusters. Finally, the applicability of the approximation to extended systems interesting in the context of the nanopolaritonic and nano-optical applications was demonstrated on the example of the light propagation and the simulation of the near-field electric field distribution in the triangular-shaped array consisting of six Ag_8 clusters.

Out approach can be easily extended to other, more accurate, quantum-chemical methods which can provide excited-state energies and transition dipole moments of the individual clusters. It can be applied to any spatial distribution (not necessarily symmetric or planar) of clusters, and the approximate self-consistent method can be used for extended systems in case the intercluster distance is kept large enough. Moreover, since the external laser field enters the calculation directly as a perturbation to the excitonic or single-cluster Hamiltonians, both methods are straightforwardly applicable to the simulation of coherent control experiments. Thus, our methods should in the future allow us to simulate the nano-optical properties of systems built from molecular-sized metal particles. Such systems are promising building blocks for the next generation of nano-optical sensors and light-harvesting systems.

ACKNOWLEDGMENTS

The authors are grateful to the Deutsche Forschungsgemeinschaft (DFG) for the financial support via the Emmy-Noether program (MI-1236) and the Priority program "Ultrafast Nanooptics" (SPP 1391).

[1] A. Sanchez, S. Abbet, U. Heiz, W. D. Schneider, H. Hakkinen, R. N. Barnett, and U. Landman, J. Phys. Chem. A **103**, 9573 (1999).
[2] A. N. Shipway, E. Katz, and I. Willner, Chem. Phys. Chem. **1**, 18 (2000).
[3] V. Bonačić-Koutecký, V. Veyret, and R. Mitrić, J. Chem. Phys. **115**, 10450 (2001).
[4] L. A. Peyser, A. E. Vinson, A. P. Bartko, and R. M. Dickson, Science **291**, 103 (2001).
[5] J. Zheng, C. W. Zhang, and R. M. Dickson, Phys. Rev. Lett. **93**, 077402 (2004).
[6] T. Lee, J. Gonzales, J. Zheng, and R. Dickson, Acc. Chem. Res. **37**, 534 (2005).
[7] S. Lal, S. Link, and N. J. Halas, Nat. Photonics **1**, 641 (2007).
[8] G. E. Johnson, R. Mitrić, V. Bonačić-Koutecký, and J. A. W. Castleman, Chem. Phys. Lett. **475**, 1 (2009).
[9] S. A. Patel, M. Cozzuol, J. M. Hales, C. I. Richards, M. Sartin, J.-C. Hsiang, T. Vosch, J. W. Perry, and R. M. Dickson, J. Phys. Chem. C **113**, 20264 (2009).
[10] P. G. Lisinetskaya and R. Mitrić, Phys. Rev. A **83**, 033408 (2011).
[11] N. Halas, S. Lal, W. Chang, S. Link, and P. Nordlander, Chem. Rev. **111**, 3913 (2011).
[12] O. Benson, Nature (London) **480**, 193 (2011).
[13] S. M. Lang and T. M. Bernhardt, Phys. Chem. Chem. Phys. **14**, 9255 (2012).
[14] S. Link and M. A. El-Sayed, J. Phys. Chem. B **103**, 8410 (1999).
[15] T. R. Jensen, M. D. Malinsky, C. L. Haynes, and R. P. Van Duyne, J. Phys. Chem. B **104**, 10549 (2000).
[16] K. L. Kelly, E. Coronado, L. L. Zhao, and G. C. Schatz, J. Phys. Chem. B **107**, 668 (2003).
[17] P. K. Jain, K. C. Lee, I. H. El-Sayed, and M. A. El-Sayed, J. Phys. Chem. B **110**, 7238 (2006).

[18] S. Nie and S. R. Emory, Science **275**, 1102 (1997).
[19] F. Tam, G. P. Goodrich, B. R. Johnson, and N. J. Halas, Nano Lett. **7**, 496 (2007).
[20] S. A. Maier, M. L. Brongersma, P. G. Kik, S. Meltzer, A. A. G. Requicha, and H. A. Atwater, Adv. Mater. **13**, 1501 (2001).
[21] M. Quinten, A. Leitner, J. R. Krenn, and F. R. Aussenegg, Opt. Lett. **23**, 1331 (1998).
[22] A. Ono, J. Kato, and S. Kawata, Phys. Rev. Lett. **95**, 267407 (2005).
[23] P. Alitalo, C. Simovski, A. Viitanen, and S. Tretyakov, Phys. Rev. B **74**, 235425 (2006).
[24] J. R. Lakowicz, Plasmonics **1**, 5 (2006).
[25] J. N. Anker, W. P. Hall, O. Lyandres, N. C. Shah, J. Zhao, and R. P. Van Duyne, Nat. Mater. **7**, 442 (2008).
[26] S. M. Morton, D. W. Silverstein, and L. Jensen, Chem. Rev. **111**, 3962 (2011).
[27] R. Mitrić, M. Hartmann, B. Stanca, V. Bonačić-Koutecký, and P. Fantucci, J. Phys. Chem. A **105**, 8892 (2001).
[28] V. Bonačić-Koutecký, J. Burda, M. Ge, R. Mitrić, G. Zampella, and R. Fantucci, J. Chem. Phys. **117**, 3120 (2002).
[29] J. Stanzel, M. Neeb, W. Eberhardt, P. G. Lisinetskaya, J. Petersen, and R. Mitrić, Phys. Rev. A **85**, 013201 (2012).
[30] H. Ma, F. Gao, and W. Z. Liang, J. Phys. Chem. C **116**, 1755 (2012).
[31] M. Aeschlimann, M. Bauer, D. Bayer, T. Brixner, F. J. Garcia de Abajo, W. Pfeiffer, M. Rohmer, C. Spindler, and F. Steeb, Nature (London) **446**, 301 (2007).
[32] M. Aeschlimann, M. Bauer, D. Bayer, T. Brixner, S. Cunovic, F. Dimler, A. Fischer, W. Pfeiffer, M. Rohmer, C. Schneider, F. Steeb, C. Strueber, and D. V. Voronine, Proc. Natl. Acad. Sci. USA **107**, 5329 (2010).
[33] S. A. Maier, P. G. Kik, and H. A. Atwater, Phys. Rev. B **67**, 205402 (2003).
[34] S. K. Gray and T. Kupka, Phys. Rev. B **68**, 045415 (2003).
[35] M. Sukharev and T. Seideman, Nano Lett. **6**, 715 (2006).
[36] T. Brixner, F. J. García de Abajo, J. Schneider, and W. Pfeiffer, Phys. Rev. Lett. **95**, 093901 (2005).
[37] H. Wang and S. Zou, Phys. Chem. Chem. Phys. **11**, 5871 (2009).
[38] B. Willingham and S. Link, Opt. Express **19**, 6450 (2011).
[39] D. Solis, B. Willingham, S. L. Nauert, L. S. Slaughter, J. Olson, P. Swanglap, A. Paul, W.-S. Chang, and S. Link, Nano Lett. **12**, 1349 (2012).
[40] M. I. Stockman, S. V. Faleev, and D. J. Bergman, Phys. Rev. Lett. **88**, 067402 (2002).
[41] M. I. Stockman, D. J. Bergman, and T. Kobayashi, Phys. Rev. B **69**, 054202 (2004).
[42] R. W. Ziolkowski, J. M. Arnold, and D. M. Gogny, Phys. Rev. A **52**, 3082 (1995).
[43] G. Slavcheva, J. M. Arnold, I. Wallace, and R. W. Ziolkowski, Phys. Rev. A **66**, 063418 (2002).
[44] A. Fratalocchi, C. Conti, and G. Ruocco, Phys. Rev. A **78**, 013806 (2008).
[45] K. Lopata and D. Neuhauser, J. Chem. Phys. **131**, 014701 (2009).
[46] M. Sukharev and A. Nitzan, Phys. Rev. A **84**, 043802 (2011).
[47] O. Christiansen, H. Koch, and P. Jorgensen, Chem. Phys. Lett. **243**, 409 (1995).
[48] R. P. Feynman, R. B. Leighton, and M. L. Sands, *The Feynman Lectures on Physics: Mainly Electromagnetism and Matter* (Addison-Wesley, Boston, 1963).
[49] U. Werner, R. Mitrić, and V. Bonačić-Koutecký, J. Chem. Phys. **132**, 174301 (2010).
[50] M. E. Casida, in *Recent Advances in Density Functional Methods*, edited by D. P. Chong (World Scientific, Singapore, 1995), p. 155.
[51] A. Dreuw and M. Head-Gordon, Chem. Rev. **105**, 4009 (2005).
[52] R. Mitrić, U. Werner, and V. Bonačić-Koutecký, J. Chem. Phys. **129**, 164118 (2008).
[53] A. D. Becke, Phys. Rev. A **38**, 3098 (1988).
[54] C. Lee, W. Yang, and R. G. Parr, Phys. Rev. B **37**, 785 (1988).
[55] A. Schäfer, C. Huber, and R. Ahlrichs, J. Chem. Phys. **100**, 5829 (1994).
[56] D. Andrae, U. Häussermann, M. Dolg, and H. Preuss, Theor. Chem. Acta **77**, 123 (1990).
[57] R. Ahlrichs, M. Bär, M. Häser, H. Horn, and M. Kölmel, Chem. Phys. Lett. **162**, 165 (1989).
[58] F. Furche and D. Rappoport, in *Computational Photochemistry*, Theoretical and Computational Chemistry, edited by M. Olivucci (Elsevier, Amsterdam, 2005), Vol. 16, Chap. 3.
[59] C. Hattig, J. Chem. Phys. **118**, 7751 (2003).
[60] C. Hattig and A. Kohn, J. Chem. Phys. **117**, 6939 (2002).